Joule

CellPress

Article

A high-performing single-stage invert-structured solar water purifier through enhanced absorption and condensation

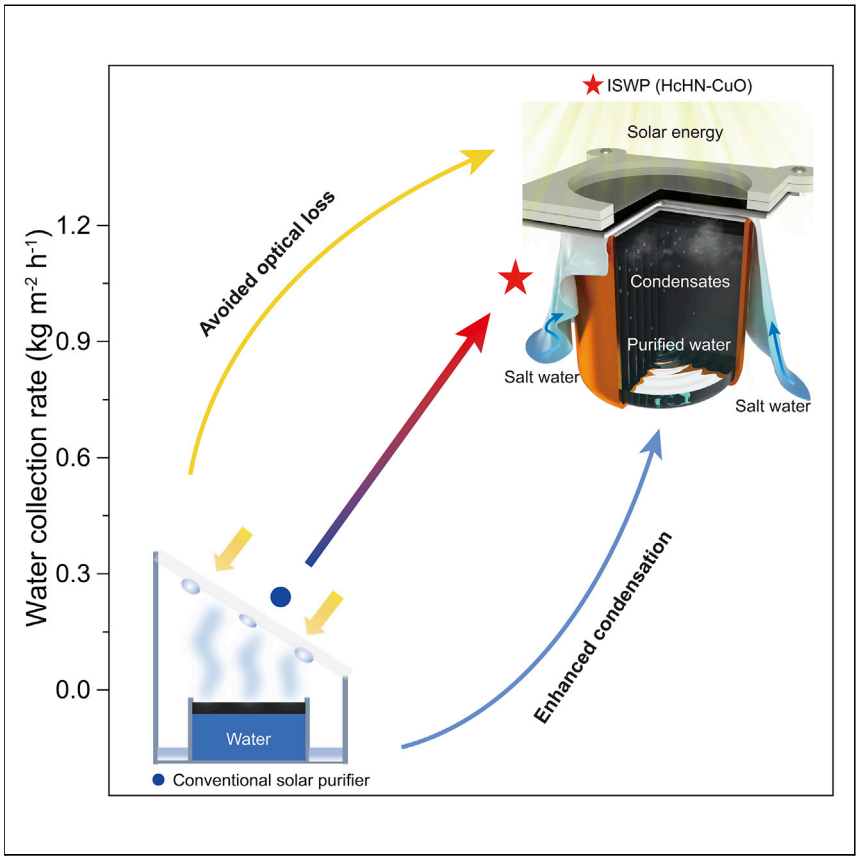

Solar water purification devices have suffered from low water production rates due to optical loss and inefficient condensation. We developed an invert-structured single-stage solar water purifier consisting of a top selective absorber and a honeycombed bottom water condenser based on hydrophobic nanostructured copper. Owing to minimized optical loss as well as enhanced heat transfer and condensation, this inverted device achieves a high water-collection rate of 1.063 kg m^{-2} h^{-1}, among the highest values for the single-stage solar water purifiers.

Fengyue Wang, Ning Xu, Wei Zhao, ..., Xueyang Wang, Bin Zhu, Jia Zhu

nxu@nju.edu.cn (N.X.)
jiazhu@nju.edu.cn (J.Z.)

Highlights

Develop a high-performing single-stage solar purifier with enhanced condensation

Realize a water-collection rate of 1.063 kg m^{-2} h^{-1} under 1-sun illumination

Provide understanding of mass and heat transfer for evaporation-condensation process

Wang et al., Joule 5, 1–11
June 16, 2021
https://doi.org/10.1016/j.joule.2021.04.009

Please cite this article in press as: Wang et al., A high-performing single-stage invert-structured solar water purifier through enhanced absorption and condensation, Joule (2021), https://doi.org/10.1016/j.joule.2021.04.009

Joule

CellPress

Article

A high-performing single-stage invert-structured solar water purifier through enhanced absorption and condensation

Fengyue Wang,[1,2] Ning Xu,[1,2,*] Wei Zhao,[1] Lin Zhou,[1] Pengcheng Zhu,[1] Xueyang Wang,[1] Bin Zhu,[1] and Jia Zhu[1,3,*]

SUMMARY

Interfacial solar vapor generation is an emerging technology for producing purified water with a minimized carbon footprint. While the evaporation rate has been significantly increased, the rate of water collection has been limited because of ineffective heat transfer during condensation and compromised light absorption in the conventionally designed solar still. In this work, an invert-structured, single-stage solar water purifier (ISWP) is elaborately designed and fabricated and consists of a top selective absorber and a honeycombed bottom water condenser based on hydrophobic nanostructured copper. This inverted structure not only avoids optical loss due to the vapor condensation but also realizes enhanced heat transfer and condensation. As a result, it can achieve a high water-collection rate of 1.063 kg m^{-2} h^{-1} and an overall efficiency of solar collected water of ~70% for single-stage solar purification systems.

INTRODUCTION

Rapid population growth and industrialization call for sustainable technologies for water treatment.[1–3] Interfacial solar-vapor generation has attracted tremendous attention as a promising water-purification process with a minimized carbon footprint. The past few years have witnessed significant progress in improving evaporation rates through designs of materials and structures.[4–7] Several materials with broad solar-absorption characteristics, such as metal nanomaterials,[8–10] carbon-based materials,[11–14] polymers,[15,16] etc., and effective thermal management strategies have been used for efficient solar-steam generation.[17–24] However, the water-collection rate is limited by inefficient condensation and is typically only 0.3–0.5 kg m^{-2} h^{-1}.[25] There are important developments to recycle the enthalpy released during vapor condensation through the multistage process or for electricity generation.[26–28] However, for on-site personalized water solutions, it is critical to improve the efficiency and water collection of the single-stage solar purifier.

Most, if not all, of previous single-stage solar purifiers typically use the single- or double-sloped structure with a transparent cover placed above a solar evaporator for both sunlight transmission and vapor condensation.[29–31] However, there are several intrinsic limitations related to this type of structure. First, the vapor mist condensed on the cover typically leads to a high optical loss (up to 35%) for the system.[32] Moreover, because of the requirements of optical transparency, the top covers are typically made of polymers or glass. These materials usually possess a low thermal conductivity κ ($\kappa < 5$ W m^{-1} K^{-1}),[33–35] which is ineffective for heat transfer related to condensation. Besides, the condensates on the cover also act as

Context & scale

Interfacial solar steam generation is regarded as a promising strategy for addressing water scarcity with minimized carbon footprint. While the past few years have witnessed significant progress in improving evaporation rates, water-collection rates have often been limited by ineffective condensation and compromised light absorption in the conventional designed solar still. Herein, we developed an invert-structured single-stage solar water purifier (ISWP), which consists of a top selective absorber and a honeycombed bottom water condenser based on hydrophobic nanostructured copper. As the ISWP device not only avoids optical loss but also realizes enhanced heat transfer and condensation, it achieves the overall efficiency of solar to collected water of ~70%. This work highlights the significance of system-level design for solar-driven water purification and provides more understanding for the mass and heat transfer of the complete evaporation-condensation process.

Please cite this article in press as: Wang et al., A high-performing single-stage invert-structured solar water purifier through enhanced absorption and condensation, Joule (2021), https://doi.org/10.1016/j.joule.2021.04.009

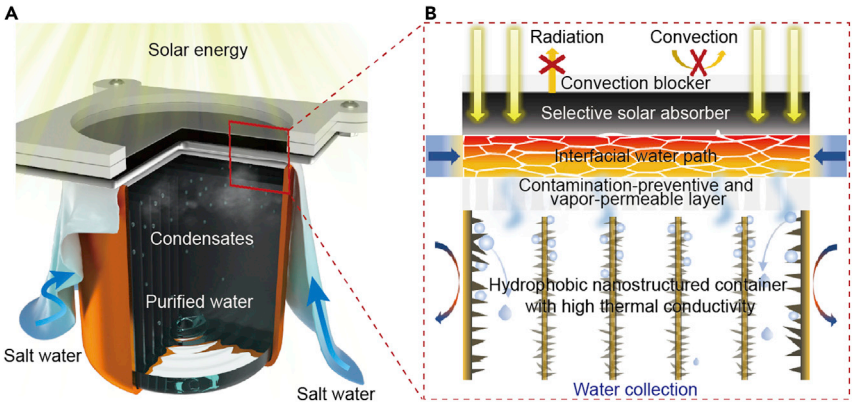

Figure 1. The design of the invert-structured solar water purifier (ISWP)

(A) Set-up diagram. The device from top to bottom consists of the convection blocker, a selective solar absorber, a water-supply layer, a contamination-preventive and vapor-permeable layer, and a bottom condenser with multiple built-in condensing walls.

(B) The schematic diagram for the process of solar water purification. The solar light transmits through the convection blocker and is captured and converted into heat by the selective absorber; the heat is transferred to evaporate the water within the hydrophilic layer; the generated vapor penetrates through the contamination-preventive and vapor-permeable layer and is condensed in the bottom condenser.

thermal barriers,[36,37] further hindering the condensation. Consequentially, the overall efficiency of solar to collected water is only ~35%, which is equivalent to ~0.5 kg m^{-2} h^{-1}.[32,38,39]

Herein, we demonstrate an invert-structured solar water purifier (ISWP) with the significantly enhanced overall efficiency of solar-collected water because of several unique features. (1) The generated vapor is driven by the vapor-pressure gradient to go downward and condensed in the bottom collector, which avoids the optical loss. (2) Without the requirement of transparency, the bottom water collector can be composed of honeycombed structures of highly thermal-conductive materials with hydrophobic nanostructures, realizing preferred dropwise condensation. (3) The inverted condenser made up of highly thermal-conductive materials can transfer the latent heat to the outside through effective heat conduction, which is beneficial for the condensation process. Thus, this inverted system can achieve a water-collection rate of 1.063 kg m^{-2} h^{-1} and overall efficiency of solar to collected water of ~70%, which is high-performing among single-stage solar-purification systems.

RESULTS AND DISCUSSION

Design of the invert-structured solar water purifier (ISWP)

Figure 1 demonstrates the set-up diagram of an ISWP from top to bottom, mainly consisting of a convection blocker, a selective solar absorber, a water-supply layer, a contamination-preventive and vapor-permeable layer, and a bottom condenser. Once the solar light transmits through the convection blocker, it is absorbed and converted into heat by the selective absorber. The heat evaporates water supplied by the confined water path. The generated vapor is then driven by the vapor-pressure gradient to go downward through the contamination-preventive and vapor-permeable layer and ultimately condensed in the bottom condenser.

In order to achieve high overall efficiency and water collection, there are a few requirements for each part of the system. (1) The convection blocker, placed above

[1]National Laboratory of solid state microstructures, Collaborative Innovation Center of Advanced Microstructures, College of Engineering and Applied Sciences, Jiangsu Key Laboratory of Artificial Functional Materials, Nanjing University, Nanjing 210093, P.R. China

[2]These authors contributed equally

[3]Lead contact

*Correspondence: nxu@nju.edu.cn (N.X.), jiazhu@nju.edu.cn (J.Z.)

https://doi.org/10.1016/j.joule.2021.04.009

Please cite this article in press as: Wang et al., A high-performing single-stage invert-structured solar water purifier through enhanced absorption and condensation, Joule (2021), https://doi.org/10.1016/j.joule.2021.04.009

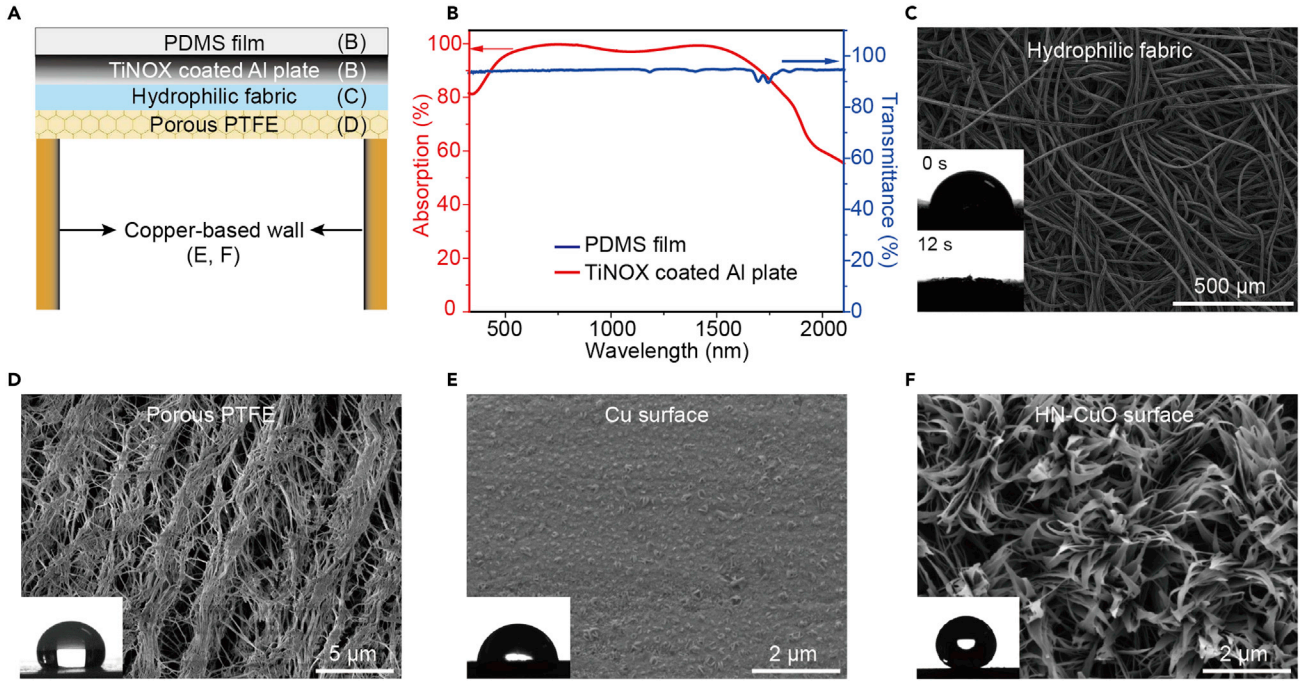

Figure 2. Characterizations of the ISWP layer by layer

(A) Layers of PDMS film, TiNOX-coated Al plate, hydrophilic fabric, porous PTFE, and copper-based wall, which are characterized, respectively, in (B–F).

(B) The transmittance spectrum of the PDMS based convection blocker and absorbance spectrum of the selective absorber (TiNOX) at wavelengths from 330 to 2,100 nm.

(C) The scanning electron microscopy (SEM) image of hydrophilic fabrics. The insets are the microscopic images of the droplet when it is dripped on the fabric.

(D) The SEM image and the contact angle (inset) of the contamination-preventive and vapor permeable layer (PTFE membrane).

(E and F) SEM images and contact angles of the smooth copper surface (E) and hydrophobic nano-structuring CuO (HN–CuO) surface (F) for the condenser.

the solar absorber, needs to possess high light transmittance and ultralow thermal convection for minimizing the optical and convective losses for the system. (2) The selective absorber needs to have high absorption of the solar spectrum and meanwhile low emittance of the infrared band, for maximizing energy input. (3) The water-supply layer should have good wettability for effective water supply from the water source. (4) The contamination-preventive and vapor-permeable layer needs to ensure sufficient vapor transport while preventing brine dripping. (5) High thermal conductance is desirable for the bottom condenser to transfer the condensation heat effectively. (6) Multiple built-in condensing walls for reducing the distance of vapor transportation.

Characterizations of each part of the ISWP

Each part of the ISWP has been elaborately designed and fabricated to meet all the requirements mentioned above (Figure 2A). The convection blocker for minimizing the convective losses (Figure S1) is made up of a 2mm-thick air layer (0.023 W m^{-1} K^{-1}) enclosed by transparent olydimethylsiloxane (PDMS) film and two 3D-printed photo-curable resin holders. The PDMS film shows a high light transmittance (~94% for the solar spectrum, 330–2100nm) (Figure 2B). TiNOX-coated aluminum plate is used as a selective solar absorber due to its high solar-spectrum-weighed absorption (~95%) (Figure 2B) and low emittance for the infrared band (~0.002% from 2.5 to 15 μm) (Figure S2; Table S1). As shown in Figure 2C, the confined water path is made up of hydrophilic fibrous fabric, which can enable fast water supply by

Please cite this article in press as: Wang et al., A high-performing single-stage invert-structured solar water purifier through enhanced absorption and condensation, Joule (2021), https://doi.org/10.1016/j.joule.2021.04.009

capillary force (Figure S3). Figure 2D demonstrates that the PTFE has an average pore size of 5 μm and a contacting angle of 106.1°, which is chosen as the contamination-preventive and vapor-permeable layer to enable effective vapor pass while preventing brine from dripping into the condenser.

The bottom condenser and built-in condensing walls are the key components to enable effective heat transfer and therefore condensation. Copper, with its high thermal conductivity (κ of 404 W $m^{-1}K^{-1}$), is chosen for effective heat transfer related to condensation. Subsequent nanostructuring and hydrophobic treatment on the surface of the condenser are used to further promote dropwise condensation.[40] Lowering the thermal resistance induced by the condensed water on the condenser wall (κ of 0.6 W $m^{-1}K^{-1}$) and accelerating the heat-transfer rate in the diffusion layer due to the existence of noncondensable gas close to the condensation surface, hydrophobized nanostructured copper-oxide (HN–CuO) film is constructed on the wall to accelerate the removal of condensate droplet and enhance the disturbance in the diffusion layer.[41,42] It is observed that the original smooth surface of Cu (Figure 2E) is transformed into knife-like nanoplates by chemical etching (Figure 2F). Meanwhile, the contact angle is significantly increased from 84.6° to 155.6° via subsequent molecular-scale surface modification, indicating the hydrophobicity of the HN–CuO surface (see experimental details and Figure S4).

Solar water production of the ISWP

To evaluate the performance of the ISWP, the yields of purified water under 1-sun illumination over time are carefully recorded. The yields of a conventional solar water purifier made of polymethyl methacrylate (PMMA) are also tested for comparison. The schematics and photos of the two devices are shown in Figures 3A and S5. Compared with the conventional purifier, the ISWP with hollow copper condenser (ISWP (Cu)) has a much higher (119% more) yield of purified water (Figure 3B).) It is confirmed that the ISWP enables higher water production, which can be ascribed to the following two reasons. (1) The vapor of ISWP is condensed in the bottom condenser to prevent the block of sunlight, which is unavoidable for the conventional design with a top light-transmitting cover for vapor condensation (Figure S6). (2) The condensation wall (the wall of the condenser) located below the absorber is made up of highly thermal-conductive copper with thermal conductivity of 404 W m^{-1} K^{-1}, which can transfer the latent heat not only by convection and radiation to ambient, but also by more efficient heat conduction when it is placed on the heat sink (Figure S7).

Besides the thermal conductivity (κ) of the condensation wall, condensate droplets also have a significant impact on the condensation process. The condensed water layer on the surface has a thermal conductivity of 0.6 W $m^{-1}K^{-1}$ and acts as a thermal barrier for transferring heat out. Furthermore, the diffusion layer due to the existence of noncondensable gas has adverse effects on mass and heat transfer in condensation. It is expected that introducing hydrophobic nanostructures can promote dropwise condensation and, therefore, enhance the disturbance in the diffusion layer, lower the thermal barrier of condensates, and lead to improved condensation performance. Consequentially, an ISWP with hydrophobic nanostructures on condenser surfaces (ISWP (HN–CuO)) shows better water-production performance than ISWP (Cu), as demonstrated in Figure 3C. It needs to be noted that the condensation condition of the ISWP contains most of the noncondensable gas (air), where the effect of hydrophobic nanostructured CuO is weakened, leading to limited enhancement of the condensation rate (Figure S8). Under a low-pressure condition, the hydrophobic effect is proved to be further enhanced (Figure S9). The ISWP device also has

Please cite this article in press as: Wang et al., A high-performing single-stage invert-structured solar water purifier through enhanced absorption and condensation, Joule (2021), https://doi.org/10.1016/j.joule.2021.04.009

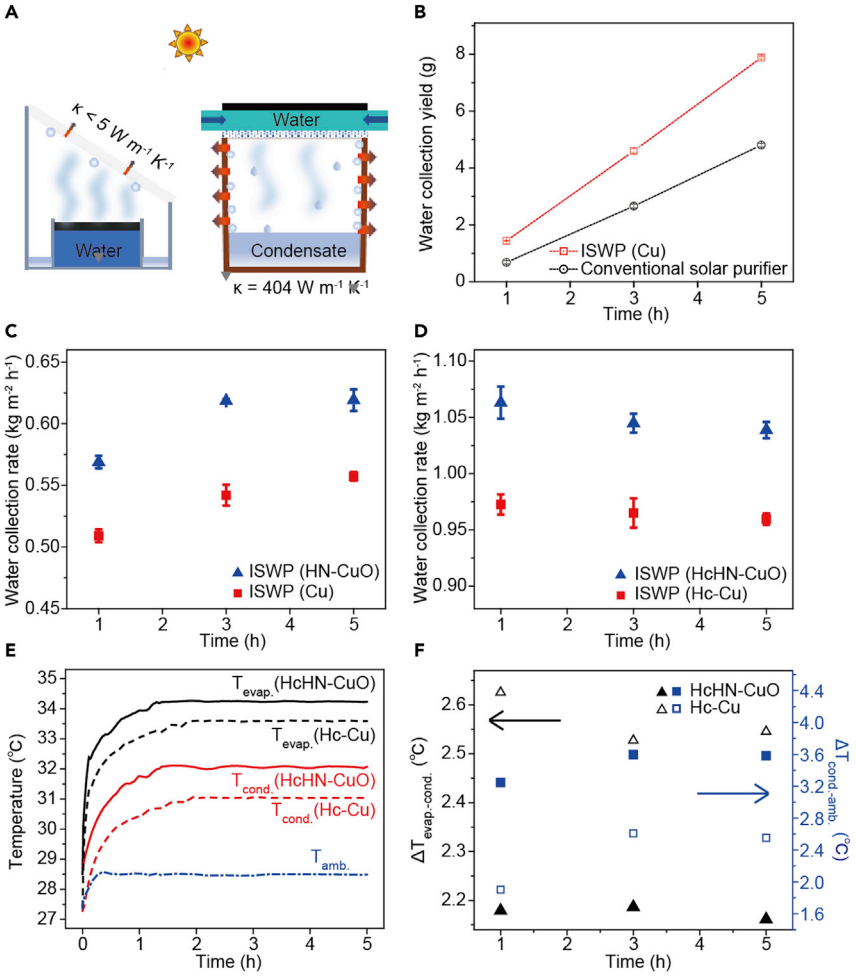

Figure 3. Water production performances and heat behaviors

(A) Device diagrams of the conventional and invert-structured solar water purifiers (ISWPs).

(B) Yields of the purified water for the ISWP (Cu) after working for 1, 3, and 5 h. The performance of a conventional solar water purifier is also tested for comparison.

(C) Water production rates over time for ISWP (Cu) and ISWP (HN–CuO). The error bars denote standard deviations, obtained by multiple experimental measurements.

(D) Water production rates over time for ISWPs with more built-in condensing walls, which are denoted as ISWP (Hc–Cu) and ISWP (HcHN–CuO). The error bars denote standard deviations, obtained by multiple experimental measurements.

(E) Temperature evolutions of the evaporators and the condensing walls for the ISWPs during a 5-h test.

(F) The respective temperature differences between the evaporating surfaces and the condensing walls as well as those between condensing walls and the ambient for the ISWP (Hc–Cu) and ISWP (HcHN–CuO).

comparable high solar-water conversion efficiency under 0.5- and 1.5-sun irradiation (Figure S10), demonstrating its adaptability in practical applications.

Vapor-transport resistance between evaporator and condenser has a great impact on the condensation performance as well. In our ISWP, embedding more effective condensation areas helps to shorten the distance between the evaporator and the condensing walls and lowering the vapor-transport resistance, beneficial for enhanced condensation performance (Note S1). Here, we construct honeycombed

ISWPs, denoted as ISWP (Hc–Cu) and ISWP (HcHN–CuO), respectively (Figure S11) with many built-in condensing walls, which show excellent performance in water production (Figure 3D). ISWP (HcHN–CuO) achieves the highest water-collection rate, as high as 1.063 kg m^{-2} h^{-1} (at 1 sun), realizing an overall solar water-collection efficiency of over 70%. The step-by-step enhancements of the water-collection rate for the ISWP systems are also demonstrated in Figure S12.

Heat behaviors of the ISWP

For understanding the condensation heat-transfer process of the ISWP, we characterize the heat behaviors of the ISWP (Hc–Cu) and ISWP (HcHN–CuO) by recording the real-time temperature evolutions for the evaporators (vapor), the condensing walls, and the ambient during the 5-h test (Figure 3E). After about 1.5 h, the two purifiers reach steady states, showing different equilibrium temperatures. The temperature differences of the vapor and condensing walls, and those of the condensing walls and ambient for the ISWP (Hc–Cu) and ISWP (HcHN–CuO) are extracted as significant data for analyzing and comparing their condensation heat transfer process (Figure 3F). The condensation heat flow can be analyzed by the equation $q = \frac{\Delta T}{R}$ (q, ΔT, and R indicate the heat flow, temperature difference, and thermal resistance, respectively). For ISWP (Hc–Cu) and ISWP (HcHN–CuO) with the same equivalent thermal resistance of convective, conductive, and radiant heat transfer from the condensing walls to the ambient, a larger temperature difference between the condensing walls and ambient of the ISWP (HcHN–CuO) indicates that more condensation heat is transferred to the ambient, which is consistent with the result that ISWP (HcHN–CuO) produces more clean water. Meanwhile, a smaller temperature difference is observed between vapor and condensing wall for ISWP (HcHN–CuO), deducing that the thermal resistance of the diffusion layer and condensed water has been indeed greatly decreased after introducing the hydrophobic nanostructures. More detailed thermal analysis can be found in Figure S13. The improvement of each process by structures/materials design for enhancing solar purification is also summarized in Figure S14.

Utility and stability of the ISWP

To test the practical applications of the ISWP, seawater (collected from the Bohai Sea) with a salinity of 1 wt % as the water source is used for solar desalination. During the 5-h test, it demonstrates a comparable yield of water production for seawater with that for pure water (Figure 4A). The purification effect for the ISWP is also evaluated by carefully tracking the ion concentrations in condensed water via inductively coupled plasma optical emission spectroscopy (ICP-OES), which has an accuracy of 0.1 mg l^{-1}. It is found that the concentrations of all the primary ions in seawater (Na^+, B^{3+}, Ca^{2+}, and Mg^{2+}) are significantly reduced, meeting the World Health Organization (WHO) standard for drinking water (Figure 4B).[43] The concentrations of Ca^{2+} and Mg^{2+} are well below the detection limit of the ICP-OES.

The ISWP device operates stably during the cycling of solar desalination. This can be ascribed to the good antisalt performance due to salt diffusion along with the water path layer. It can be seen that no salt accumulation occurs during a 12-h test, even when using 7 wt % NaCl aqueous solution as the water source (Figure S15). Moreover, as we put salt of 0.2 g (roughly corresponding to the amount of salt-accumulation during 12-h water treatment of 1 wt % brine), the salt can be diffused back to the bulk water via hydrophilic fabric during 8-h of dark time. Thus, the solar desalination performance for the ISWP (HN–CuO) remains stable over 8 cycles, each cycle lasting for 12 h (Figure 4C). As shown in Figure 4D, the rate of solar-powered clean water collection for this invert-structured design is higher than most if not all of the

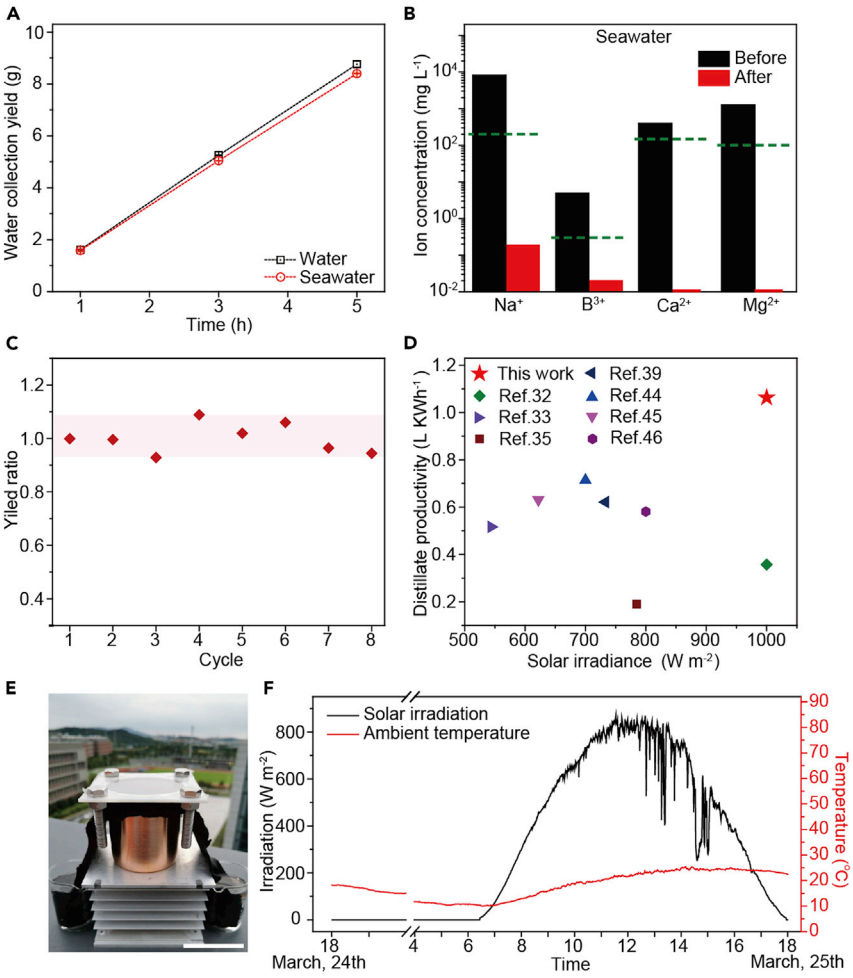

Figure 4. Desalination performance for the ISWP

(A) Yields of water production for the ISWP(HN–CuO) over time when treating seawater. It shows yields from treating seawater to those of treating pure water; the seawater was collected from the Bohai Sea, China, with an average salinity of ~1 wt %.

(B) Ion concentrations before and after water purification. The dash green lines show the WHO standard of ion concentrations for drinking water.

(C) Stability of the desalination performance for the ISWP (HN–CuO) over time (normalized with the average yield, 20.72 g).

(D) Comparison of the performances for the optimized ISWP with other reported single-stage solar purification systems.

(E) Optical photo of the ISWP prototype. Scale bar: 6 cm.

(F) Environmental conditions (temperature and solar irradiation intensity) during the outdoor experiment.

reported single-stage solar purification systems,[32,33,35,39,44–46] because of the unique structural design with minimized optical loss and enhanced condensation.

To further demonstrate the performance in its practical application, an outdoor experiment was conducted on the roof at Nanjing University (Nanjing, Jiangsu province, China) from March 24th and 25th, 2021 (Figure 4E). The ambient temperature and real-time solar irradiation during the experiment are recorded by a meteorological station, as shown in Figure 4F. The solar irradiation varied from 0 to 866 W m^{-2} due to the scattered clouds and the total insolation is 5.61 KWh m^{-2} day^{-1}. The water production rates of ISWP (HN–CuO) and ISWP (HcHN–CuO) were 4.09 and 5.40 kg m^{-2} day^{-1},

demonstrating their good performance under practical conditions. We also estimate the total material costs of the ISWP device (Figure S16; Table S2), which is about $\$25/m^2$.

Conclusion

In summary, we reported an ISWP with enhanced condensation and minimized optical loss, which achieves a water production rate of 1.063 kg m^{-2} h^{-1}, and the overall efficiency of the solar water collection is over 70%. With structural innovations and significantly enhanced water-collection rates, it provides a promising pathway toward portable or personalized clean-water production in water-deficient or wild areas. The innovative treatment of the condensation surface in this work can also be applied to multistage devices for further enhancing their condensation efficiency.

EXPERIMENTAL PROCEDURES

Resource availability

Lead contact

Further information and requests for resources and materials should be directed to and will be fulfilled by the lead contact, Ning Xu and Jia Zhu (nxu@nju.edu.cn; jiazhu@nju.edu.cn).

Materials availability

This study did not generate unique materials.

Data and code availability

The published article includes all datasets generated or analyzed during this study.

Fabrication of the ISWP

The ISWP consists of a convection blocker, a selective absorber, hydrophilic water paths, a contamination-preventive and vapor-permeable layer, and a condenser. The convection blocker is composed of transparent PDMS film and 3D-printed acrylonitrile butadiene styrene (ABS) frame (hollow circular in the middle, the diameter is 60 mm). TiNOX-coated aluminum plate is commercially available and is cut into a size of 8 × 8 cm. The hydrophilic water path is made up of commercial hydrophilic fabric. The porous PTFE membrane is used as the contamination-preventive and vapor-permeable layer. The condenser is made up of a copper bottle with a diameter of 6 cm. The convection blocker was stuck to the TiNOX-coated plate.

Fabrication of the HN–CuO surface

The nanostructures on the surface of the copper bottle were prepared by filling up with a mixture of $NaClO_2$, NaOH, $Na_3PO_4 \cdot 12H_2O$, and DI water (3.75:5:10:100 wt %), which was already heated to ~98°C. The liquid mixture was removed after 10 min. The internal wall of the copper bottle was cleaned by clean water for several times. Then, the bottle was filled up with a solution of 1H,1H,2H,2H-perfluorooctyltrichloro silane dissolved in methyl alcohol with a concentration of 2 vol %. The liquid was removed after 1 h. The bottle was baked at 145°C for 1 h.

Fabrications of the conventional solar water purifier

The conventional solar water purifier is made of PMMA with the following parameters: 10.5-cm length, 10.5-cm breadth, 13.0-cm height, the thickness and tip angle of the top cover is 1.5 mm and 45°, respectively.

Characterizations of the ISWP

The absorption and emittance spectra of the selective absorber were measured by ultraviolet-visible spectroscopy (UV-3600, Shimadzu) attached with an integrating sphere (ISR-3100) and infrared spectrometer (Nicolet IS50, ThermoFisher) equipped with an integrating sphere (Model 4P-GPS-020-SL, Pike). The microscopic structures and water contact angles of the hydrophilic layer, hydrophobic membrane (PTFE), copper surface, and hydrophobic surface were characterized by a scanning electron microscope (TESCAN MIRA3) and a surface tension/contact angle meter (GBX Digidrop), respectively. The IR images of water-pumping processes were captured by an IR camera (FLUKE, Tix 580). The concentrations of cations in condensates were examined by ICP-OES (PerkinElmer Instruments, PTIMA 5300 DV). The optimized ISWP was constructed by increasing condensation areas (by adding copper-based sheets into the condensation container) and enhancing the convection (by making the device float on the bulk water for simulating the condition that the device floats on the sea).

Experimental conditions for condensation performance

A solar simulator (94043A, Newport) equipped with an optical filter for the standard AM 1.5G spectrum was used for indoor experiments of condensation performance tests and solar desalination, and the Xe lamp was used for long-cycle tests. An optical power meter is used to measure the light intensity, and a thermocouple records the temperature of the selective solar absorber, the outer wall of the bottom condenser and the ambient. During these experiments, the indoor temperature is carefully stabilized at 26.5°C $\pm$ 0.5°C. After running for specific times, the solar purifier is separated, and the yield of condensate is measured by a balance. The outdoor experiment is conducted from 6 pm March 24th to 6 pm March 25th on the roof of the Zhenjiang Building in Nanjing University (Nanjing, Jiangsu province, China). The ambient conditions (temperature, solar irradiation) are recorded by the meteorological station (Tuolaisi, TS-G1).

SUPPLEMENTAL INFORMATION

Supplemental information can be found online at https://doi.org/10.1016/j.joule.2021.04.009.

ACKNOWLEDGMENTS

We thank the Prof. Yangying Zhu for the discussion of the condensation part. We acknowledge the micro-fabrication center of National Laboratory of Solid State microstructures (NLSSM) for technical support. Prof. Jia Zhu acknowledges the support from the XPLORER PRIZE. This work is jointly supported by the National Natural Science Foundation of China (Nos. 61735008, 12022403, 51925204, 11874211, and 52002168), Natural Science Foundation of Jiangsu Province (no. BK20200340), the Fundamental Research Funds for the Central Universities (nos. 021314380179, 021314380150, and 021314380140), the National Key Research and Development Program of China (2017YFA0205700), Key Science and Technology Inovation Program of Shandong Province (2019JZZY020704).

AUTHOR CONTRIBUTIONS

J.Z. supervised the project. N.X. and F.W. designed the experiments. F.W., N.X, W.Z., P.Z., X.W., and B.Z. performed experiments. All authors discussed the experiments and results. N.X., F.W., and J.Z. prepared and revised the manuscript.

DECLARATION OF INTERESTS

The authors declare no competing interests.

Received: May 5, 2020
Revised: February 5, 2021
Accepted: April 19, 2021
Published: May 20, 2021

REFERENCES

1. Fan, X., Tao, Y., Wang, L., Zhang, X., Lei, Y., Wang, Z., and Noguchi, H. (2014). Performance of an integrated process combining ozonation with ceramic membrane ultra-filtration for advanced treatment of drinking water. Desalination *335*, 47–54.
2. Shalaby, S.M. (2017). Reverse osmosis desalination powered by photovoltaic and solar Rankine cycle power systems: a review. Renew. Sustain. Energy Rev. *73*, 789–797.
3. Oki, T., and Kanae, S. (2006). Global hydrological cycles and world water resources. Science *313*, 1068–1072.
4. Qiblawey, H.M., and Banat, F. (2008). Solar thermal desalination technologies. Desalination *220*, 633–644.
5. Zhu, L., Gao, M., Peh, C.K.N., and Ho, G.W. (2018). Solar-driven photothermal nanostructured materials designs and prerequisites for evaporation and catalysis applications. Mater. Horiz. *5*, 323–343.
6. Zhao, F., Guo, Y., Zhou, X., Shi, W., and Yu, G. (2020). Materials for solar-powered water evaporation. Nat. Rev. Mater. *5*, 388–401. https://doi.org/10.1038/s41578-020-0182-4.
7. Zhu, L., Gao, M., Peh, C.K.N., and Ho, G.W. (2019). Recent progress in solar-driven interfacial water evaporation: advanced designs and applications. Nano Energy *57*, 507–518.
8. Zhou, L., Tan, Y., Wang, J., Xu, W., Yuan, Y., Cai, W., Zhu, S., and Zhu, J. (2016). 3D self-assembly of aluminium nanoparticles for plasmon-enhanced solar desalination. Nature Photon *10*, 393–398.
9. Bae, K., Kang, G., Cho, S.K., Park, W., Kim, K., and Padilla, W.J. (2015). Flexible thin-film black gold membranes with ultrabroadband plasmonic nanofocusing for efficient solar vapour generation. Nat. Commun. *6*, 10103.
10. Zhou, L., Tan, Y., Ji, D., Zhu, B., Zhang, P., Xu, J., Gan, Q., Yu, Z., and Zhu, J. (2016). Self-assembly of highly efficient, broadband plasmonic absorbers for solar steam generation. Sci. Adv. *2*, e1501227.
11. Gao, X., Ren, H., Zhou, J., Du, R., Yin, C., Liu, R., Peng, H., Tong, L., Liu, Z., and Zhang, J. (2017). Synthesis of hierarchical graphdiyne-based architecture for efficient solar steam generation. Chem. Mater. *29*, 5777–5781.
12. Li, X., Xu, W., Tang, M., Zhou, L., Zhu, B., Zhu, S., and Zhu, J. (2016). Graphene oxide-based efficient and scalable solar desalination under one sun with a confined 2D water path. Proc. Natl. Acad. Sci. USA *113*, 13953–13958.
13. Cui, L., Zhang, P., Xiao, Y., Liang, Y., Liang, H., Cheng, Z., and Qu, L. (2018). High rate production of clean water based on the combined photo-electro-thermal effect of graphene architecture. Adv. Mater. *30*, e1706805.
14. Li, J., Wang, X., Lin, Z., Xu, N., Li, X., Liang, J., Zhao, W., Lin, R., Zhu, B., Liu, G., et al. (2020). Over 10 kg m2 h-1 evaporation rate enabled by a 3D interconnected porous carbon foam. Joule *4*, 687.
15. Zhang, L., Tang, B., Wu, J., Li, R., and Wang, P. (2015). Hydrophobic light-to-heat conversion membranes with self-healing ability for interfacial solar heating. Adv. Mater. *27*, 4889–4894.
16. Gao, M., Peh, C.K., Phan, H.T., Zhu, L., and Ho, G.W. (2018). Solar absorber gel: localized macro-nano heat channeling for efficient plasmonic Au nanoflowers photothermic vaporization and triboelectric generation. Adv. Energy Mater. *8*, 1800711.
17. Ni, G., Li, G., Boriskina, S., Li, H., Yang, W., Zhang, T., and Chen, G. (2016). Steam generation under one sun enabled by a floating structure with thermal concentration. Nat. Energy *1*, 1–7.
18. Liang, H., Liao, Q., Chen, N., Liang, Y., Lv, G., Zhang, P., Lu, B., and Qu, L. (2019). Thermal efficiency of solar steam generation approaching 100 % through capillary water transport. Angew. Chem. Int. Ed. Engl. *58*, 19041–19046.
19. Xu, N., Li, J., Wang, Y., Fang, C., Li, X., Wang, Y., Zhou, L., Zhu, B., Wu, Z., Zhu, S., and Zhu, J. (2019). A water lily–inspired hierarchical design for stable and efficient solar evaporation of high-salinity brine. Sci. Adv. *5*, eaaw7013.
20. Xu, N., Hu, X., Xu, W., Li, X., Zhou, L., Zhu, S., and Zhu, J. (2017). Mushrooms as efficient solar steam-generation devices. Adv. Mater. *29*, 1606762.
21. Chen, C., Li, Y., Song, J., Yang, Z., Kuang, Y., Hitz, E., Jia, C., Gong, A., Jiang, F., Zhu, J.Y., et al. (2017). Highly flexible and efficient solar steam generation device. Adv. Mater. *29*, 1701756.
22. Ghasemi, H., Ni, G., Marconnet, A.M., Loomis, J., Yerci, S., Miljkovic, N., and Chen, G. (2014). Solar steam generation by heat localization. Nat. Commun. *5*, 4449.
23. Li, Y., Gao, T., Yang, Z., Chen, C., Luo, W., Song, J., Hitz, E., Jia, C., Zhou, Y., Liu, B., et al. (2017). 3D-printed, all-in-one evaporator for high-efficiency solar steam generation under 1 sun illumination. Adv. Mater. *29*, 1700981.
24. Shi, Y., Li, R., Jin, Y., Zhuo, S., Shi, L., Chang, J., Hong, S., Ng, K., and Wang, P. (2018). A 3D photothermal structure toward improved energy efficiency in solar steam generation. Joule *2*, 1171–1186.
25. Dsilva Winfred Rufuss, D., Iniyan, S., Suganthi, L., and Davies, P.A. (2016). Solar stills: a comprehensive review of designs, performance and material advances. Renew. Sustain. Energy Rev. *63*, 464–496.
26. Chiavazzo, E., Morciano, M., Viglino, F., Fasano, M., and Asinari, P. (2018). Passive solar high-yield seawater desalination by modular and low-cost distillation. Nat. Sustain. *1*, 763–772.
27. Xu, Z., Zhang, L., Zhao, L., Li, B., Bhatia, B., Wang, C., Wilke, K.L., Song, Y., Labban, O., Lienhard, J.H., et al. (2020). Ultrahigh-efficiency desalination via a thermally-localized multistage solar still. Energy Environ. Sci. *13*, 830–839.
28. Li, X., Min, X., Li, J., Xu, N., Zhu, P., Zhu, B., Zhu, S., and Zhu, J. (2018). Storage and recycling of interfacial solar steam enthalpy. Joule *2*, 2477–2484.
29. Srivastava, P.K., and Agrawal, S.K. (2013). Experimental and theoretical analysis of single sloped basin type solar still consisting of multiple low thermal inertia floating porous absorbers. Desalination *311*, 198–205.
30. Arunkumar, T., Kabeel, A.E., Raj, K., Denkenberger, D., Sathyamurthy, R., Ragupathy, P., and Velraj, R. (2018). Productivity enhancement of solar still by using porous absorber with bubble-wrap insulation. J. Cleaner Prod *195*, 1149–1161.
31. Gnanaraj, S.J.P., and Velmurugan, V. (2019). An experimental study on the efficacy of modifications in enhancing the performance of single basin double slope solar still. Desalination *467*, 12–28.
32. Ni, G., Zandavi, S.H., Javid, S.M., Boriskina, S.V., Cooper, T.A., and Chen, G. (2018). A salt-rejecting floating solar still for low-cost desalination. Energy Environ. Sci. *11*, 1510–1519.
33. Gupta, B., Shankar, P., Sharma, R., and Baredar, P. (2016). Performance enhancement using Nano particles in modified passive solar still. Procedia Technol *25*, 1209–1216.
34. Pareek, V., Gupta, R., and Panwar, J. (2018). Do physico-chemical properties of silver

nanoparticles decide their interaction with biological media and bactericidal action? A review. Mater. Sci. Eng. C Mater. Biol. Appl. *90*, 739–749.

35. Jani, H.K., and Modi, K.V. (2019). Experimental performance evaluation of single basin dual slope solar still with circular and square cross-sectional hollow fins. Sol. Energy *179*, 186–194.

36. Mulroe, M.D., Srijanto, B.R., Ahmadi, S.F., Collier, C.P., and Boreyko, J.B. (2017). Tuning superhydrophobic nanostructures to enhance jumping-droplet condensation. ACS Nano *11*, 8499–8510.

37. Gose, E.E., Mucciardi, A.N., and Baer, E. (1967). Model for dropwise condensation on randomly distributed sites. Int. J. Heat Mass Transf. *10*, 15–22.

38. Velmurugan, V., Gopalakrishnan, M., Raghu, R., and Srithar, K. (2008). Single basin solar still with fin for enhancing productivity. Energy Convers. Manag. *49*, 2602–2608.

39. Kabeel, A.E. (2009). Performance of solar still with a concave wick evaporation surface. Energy *34*, 1504–1509.

40. Miljkovic, N., Enright, R., Nam, Y., Lopez, K., Dou, N., Sack, J., and Wang, E.N. (2013). Jumping-droplet-enhanced condensation on scalable superhydrophobic nanostructured surfaces. Nano Lett *13*, 179–187.

41. Ma, X., Zhou, X., Lan, Z., Li, Y., and Zhang, Y. (2008). Condensation heat transfer enhancement in the presence of non-condensable gas using the interfacial effect of dropwise condensation. Int. J. Heat Mass Transf. *51*, 1728–1737.

42. Shen, L.Y., Tang, G.H., Li, Q., and Shi, Y. (2019). Hybrid wettability-induced heat transfer enhancement for condensation with noncondensable gas. Langmuir *35*, 9430–9440.

43. WHO (2011). Guidelines for Drinking-Water Quality, 4th Edition (World Health Organization). https://www.who.int/water_sanitation_health/publications/dwq-guidelines-4/en/.

44. Dongare, P.D., Alabastri, A., Pedersen, S., Zodrow, K.R., Hogan, N.J., Neumann, O., Wu, J., Wang, T., Deshmukh, A., Elimelech, M., et al. (2017). Nanophotonics-enabled solar membrane distillation for off-grid water purification. Proc. Natl. Acad. Sci. USA *114*, 6936–6941.

45. Ahsan, A., Imteaz, M., Rahman, A., Yusuf, B., and Fukuhara, T. (2012). Design, fabrication and performance analysis of an improved solar still. Desalination *292*, 105–112.

46. Muthu Manokar, A., Prince Winston, D., Sathyamurthy, R., Kabeel, A.E., and Rama Prasath, A. (2019). Experimental investigation on pyramid solar still in passive and active mode. Heat Mass Transfer *55*, 1045–1058.